Inorganic Chemistry

pubs.acs.org/IC

Article

Proton-Coupled, Low-Energy Pathway for Electrocatalytic CO_2 Reduction at Re(Diimine) Complexes with a Conjugated Pyrazinyl Moiety

Sruthy K. Chandy,[†] Scott A. Bowers,[†] Minyang Yin, Lu Liu, Krishnan Raghavachari,* and Liang-shi Li*

Cite This: https://doi.org/10.1021/acs.inorgchem.2c02400

Read Online

ACCESS | Metrics & More | Article Recommendations | Supporting Information

ABSTRACT: Large conjugated carbon framework has been incorporated as the diimine ligand for Re(α-diimine)$(CO)_3$Cl complexes with a pyrazinyl linkage, either to increase energy efficiency or to turn them into heterogeneous catalysts for selective electrocatalytic CO_2 reduction. However, there exists a nonmonotonic dependence of CO_2 reduction overpotential on the conjugation size of the ligands. Understanding its origin could facilitate heterogenization of molecular catalysts with improved energy efficiency. Here, we show that the conjugated pyrazinyl moiety plays a crucial role in catalysis by enabling a proton-coupled, lower-energy pathway for CO_2 reduction. With ligands of moderate size, the pathway leads to previously unknown intermediates and decreases CO_2 reduction overpotential. Because the pathway hinges on the basicity of the pyrazinyl nitrogen, we propose that it imposes a limit on the conjugation size of the ligand for the pathway to be effective.

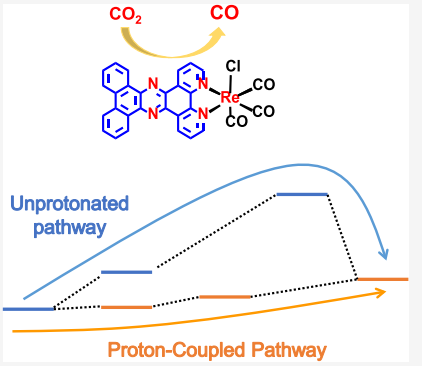

INTRODUCTION

Multielectron catalytic reactions involving small molecules or ions such as H_2O, O_2, CO_2, or NO_3^- are of great importance for utilizing sustainable energy sources and mitigating the adverse impacts of human activities.[1−4] For this purpose, homogeneous molecular catalysts, most notably those based on metal complexes, have been intensively studied because of their versatility toward various substrates and selectivity in directing chemical reactions along specific pathways. In designing such molecular catalysts, an important approach involves employing redox noninnocent ligands to match the redox potentials of the catalysts with those of the substrates.[5,6] Meanwhile, immobilization of the molecular catalysts (covalently or noncovalently) on the electrode surfaces has been investigated to combine the tunability of molecular catalysts with the advantages of heterogeneous catalysts such as higher stability, lower loading requirements, and ease in catalyst removal.[7,8]

A seemingly general approach to heterogenization was recently reported through covalently grafting molecular catalysts to the graphite surface with a pyrazinyl linkage (schematically shown as **A** in Scheme 1).[9−11] The covalent linkage enables inner-sphere electron transfer from the electrodes to the catalysts, improving the catalytic performance and could even alter the catalytic mechanisms.[11] However, when applied to *fac*-Re(α-diimine)$(CO)_3$Cl complexes,[10] a widely studied family of electrocatalysts for CO_2 reduction,[12−16] it was found that the catalyst, though it drastically improved electron transfer dynamics and catalysis turnover frequency, did not improve the CO_2 reduction overpotential compared with the well-studied, but much smaller, Re(bpy)-$(CO)_3$Cl (bpy = 2, 2′-bipyridine). In contrast, we applied a nanographene derivative as the diimine ligand for the same family of complexes (**B** in Scheme 1).[17] It significantly decreased reaction overpotential (by 0.8 V in THF), leading to one of the lowest values for CO_2 reduction to CO.[17] Based on theoretical calculations, we attributed the improvement to the increased conjugation size of the ligand, which enables ligand-centered reductions at lower applied electrochemical potentials to drive the reaction. Because **A** can be considered as an analogue of **B** with a graphene of infinite size, it raises an interesting question why there is such a nonmonotonic dependence between the conjugation size of the ligand and the reaction overpotential. Understanding the origin may provide important insights to better apply ubiquitous graphitic carbon materials as redox-active ligands to create heterogeneous electrocatalysts with tunable properties.

In this study, we aim to identify structural factors that disrupt an anticipated monotonic dependence between the conjugation size of the ligand and the reaction overpotential. By investigating **1**, a smaller analogue of **B** (Scheme 1) with combined electrochemical, spectroscopic, and theoretical

Received: July 8, 2022

Scheme 1. Structures of A, B, and 1

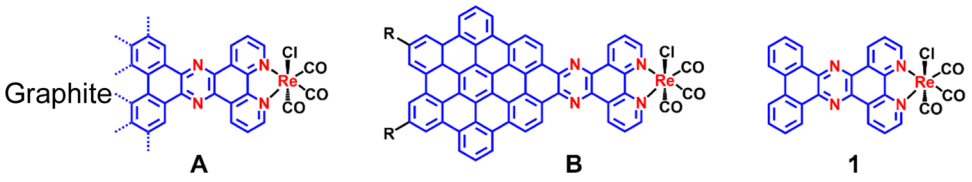

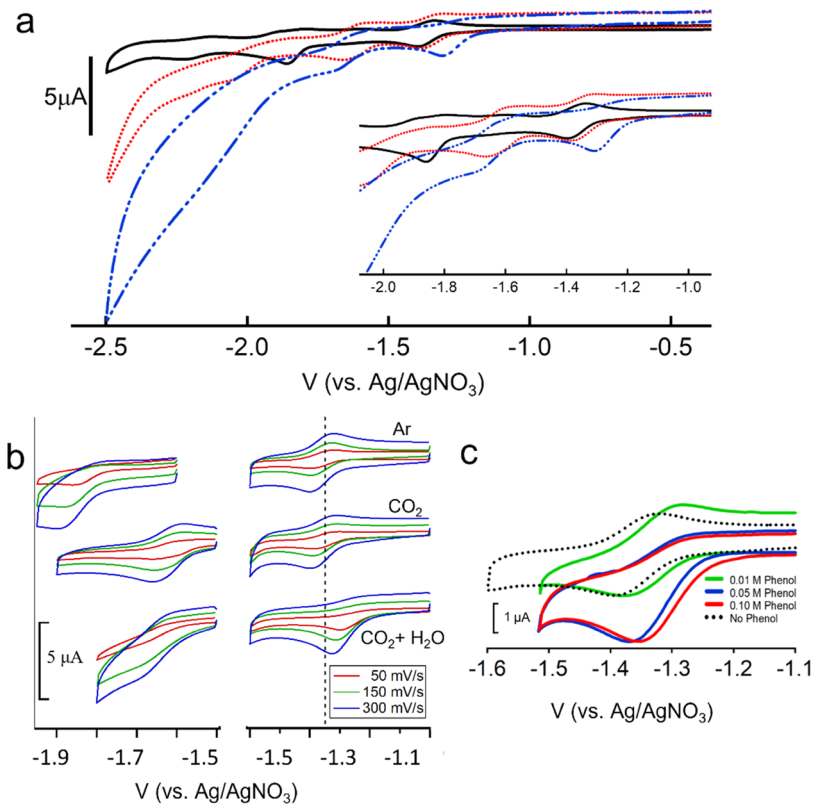

Figure 1. CV measurements of 0.10 mM solution of **1** in dry THF. (a) CV under argon (black solid curve), CO_2 (red dotted curve), and CO_2 and water (5% v/v, blue dashed curve). The inset is the zoom-in of the selected voltage range. (b) CV scans at various scan rates under the three reaction conditions. (c) CV scans with various amounts of phenol added under an argon atmosphere.

studies, we show that the pyrazinyl moiety in both **A** and **B** plays roles beyond serving as a covalent linkage. Protonation at a nitrogen atom in the pyrazinyl moiety can couple to the reduction of the catalyst, opening a previously unknown, lower-energy reaction pathway that decreases the CO_2 reduction overpotential. Thus, we propose that the decreasing basicity of the pyrazinyl nitrogen atoms with increasing conjugation size of the ligand could diminish the benefits of employing large conjugated ligands when the size reaches a certain limit. In addition, the low-energy reaction pathway revealed with heterocyclic nitrogen moieties may provide a useful approach to improve the energy efficiency of electrocatalytic reactions at metal complexes in general.

RESULTS AND DISCUSSION

Synthesis and Characterization of 1. In our study, we investigate a smaller molecular analogue **1** (Scheme 1) of **B** because of the low solubility of **B** for spectroscopic studies and the comparative difficulty for theoretical calculations due to its large size. With details described in the Supporting Information, the ligand in **1** was synthesized with a previously reported method.[18] **1** was then synthesized by reacting the ligand with freshly sublimed $Re(CO)_5Cl$ in chloroform. The product was recrystallized from THF and characterized with NMR and IR (see the Supporting Information).

Electrochemical Reduction of 1 in THF. We investigated the electrochemical properties of **1** with cyclic voltammetry (CV) in tetrahydrofuran (THF), to compare with the catalytic behaviors of **B** previously reported in the same solvent.[17] The CV measurements were conducted with a glassy carbon working electrode, a platinum auxiliary electrode, and Ag/$AgNO_3$ (0.01 M in acetonitrile) reference electrode. The solvent used was anhydrous THF freshly distilled over sodium metal, and a 0.10 M solution of freshly recrystallized tetrabutylammonium hexafluorophosphate ($TBAPF_6$) was the supporting electrolyte.

The black solid curve in Figure 1a shows the CV curve of **1** (0.10 mM, scan rate: 100 mV/s) under an argon atmosphere (1 atm). The cathodic scan reveals two distinct reduction peaks, at −1.40 and −1.90 V, respectively. Measurements with various scan rates reveal that the first reduction is reversible within the time scale of the CV scan while the second reduction is irreversible (Figures 1b and S-4). This is consistent with previous work on $Re(bpy)(CO)_3Cl$ in that the first reduction is simply an electron transfer, and the

https://doi.org/10.1021/acs.inorgchem.2c02400
Inorg. Chem. XXXX, XXX, XXX−XXX

second is concerted with dechlorination, though at less negative potentials (−1.71 and −2.18 V, respectively, for Re(bpy)(CO)$_3$Cl in THF).[19]

When CO_2 is introduced into the solution, the first reduction occurs at the same potential, whereas there is an apparent shift of the second reduction peak to a less negative potential −1.65 V (red dotted curve, Figure 1a). However, scanning at various rates revealed that both the reductions are reversible in the CV time scale. There appears to be a third reduction with the peak position at −2.10 V, beyond which a moderate current increase was observed.

Drastic changes occur when water was added (5% vol/vol) under the CO_2 atmosphere (blue dashed curve, Figure 1a). The first reduction peak shifts positive to −1.30 V, accompanied by doubling of the peak current. The second reduction appears at the same potential as in the case with no water but is immediately followed by a substantially enhanced current indicating catalytic reduction of CO_2. The CO_2 reduction onset potential of −1.70 V is about 300 mV less negative than that for Re(bpy)(CO)$_3$Cl in THF and 500 mV more than that for **B** (see comparison tabulated in Table S-1), consistent with the expected trend that a larger conjugated ligand leads to a lower overpotential. CV measurements at various scan rates showed that both reductions are irreversible. With the foot-of-wave analysis,[20,21] we obtained the turnover frequency of **1** to be 466 s^{-1} (see the Supporting Information). Bulk electrolysis with such a solution at a glassy carbon mesh with the potential held at −2.0 V and subsequent gas chromatography analysis show CO as the only product with no H_2 detected (see the Supporting Information). The faradic efficiency of **1** was measured to be 98% (±2%).

It is clear from the above observations that the presence of water as a Brønsted acid results in a different reduction mechanism, as indicated by the changes in the peak currents, the reversibility, and the peak potentials, and leads to the electrocatalytic CO_2 reduction. The first reduction peak (at −1.30 V) is consistent with either a proton-coupled reduction followed by another one-electron reduction or a proton-coupled two-electron reduction. The reduction being proton-coupled is confirmed when phenol, a stronger acid, was added as a proton source under the argon atmosphere (Figure 1c). Here, increasing the phenol concentration in the solution reproduces the first reduction occurring at increasingly positive potentials with a doubled peak current, while turning the process into an irreversible one. The second reduction at −1.65 V (blue dashed curve, Figure 1a) was better resolved by employing CV measurements with a faster scan rate (Figure S-5). They show a separate one-electron reduction step and an additional subsequent step producing the catalytic current, the latter of which presumably regenerates the catalysts and releases CO.

Calculated Electrochemical Pathways. To understand the mechanisms of CO_2 reduction catalyzed by **1** in the presence of CO_2 and water and to confirm the role of the proton-coupled reduction in the catalysis, we carried out theoretical calculations to investigate the thermodynamics of electrochemical reduction of **1** and subsequent reactions under the experimental conditions. The reactions we examined include dechlorination, dimerization, and formation of CO_2 adducts, which have been previously reported for Re(bpy)(CO)$_3$Cl and derivatives,[19,22,23] as well as protonation of pyrazinyl nitrogen suggested by the CV measurements and our previous work on the oxygen reduction reaction.[24] All of the calculations were performed with Gaussian 16[25] quantum chemical package starting from the unrestricted version of B3LYP[26−29] density functional theory (DFT). To include the van der Waals interactions for weakly bound systems, Grimme's empirical pairwise D3 dispersion correction[30] was included with Becke−Johnson damping (uB3LYP-D3BJ) in all of the calculations.[31−33] Geometry optimizations and vibrational frequency calculations on the different species were carried out in an implicit solvent-corrected potential energy surface (PES) to derive the entropies and the associated thermal corrections (at 298.15 K) to the Gibbs free energies. Conductor-like polarizable continuum model, CPCM method[34−37] was used to account for the solvation energy in all of the calculations in THF (ε = 7.25). The geometry optimizations were carried out using the def2-SVP basis set[38] for C, N, H, O, and Cl atoms while Re orbitals were modeled with def2-SVP basis set for valence electrons and Stuttgart/Dresden (SDD) effective core potential[39] for core electrons. Accurate electronic energies at these geometries were calculated using the larger def2-TZVPP basis set[40−43] with CPCM implicit solvation.

The thermal-corrected free energy of each species was determined by combining the SCF energy calculated using the large basis set def2-TZVPP and CPCM solvation corrections, zero-point energy (ZPE), and entropic contribution at 298.15 K calculated using the smaller basis set def2-SVP. That is, $G^0_{sol} = E_{SCF} + \Delta G_{CPCM} + ZPE - (298.15\ K \times S_{total})$, where $S_{total} = S_{trans} + S_{rot} + S_{vib} + S_{elec}$. All of the species were treated in the solution phase unless released in the gas phase. Translational, rotational, and vibrational contributions to entropy were obtained from the harmonic oscillator and rigid rotor approximations,[44] whereas $R \ln (q_{elec})$ gives the electronic contribution to entropy, with R as the gas constant and q_{elec} as the multiplicity of the species.

To accurately capture the effect of the THF solvent on the reduction process, an explicit THF solvent molecule was added at the open metal site of the complex after chloride loss in conjunction with the implicit solvation-corrected PES.

Broken symmetry calculations were investigated on all even electron species, by performing the initial geometry optimization with the high spin triplet state and using its optimized geometry as the starting geometry for singlet calculations.

Concentration effects are included in our calculations using the law of mass action. Accurate prediction of Gibbs free energy is obtained by combining standard Gibbs energy in solution (G^0_{sol}) and concentration corrections, e.g., $\Delta G_{sol} = \Delta G^0_{sol} + RT \ln\left(\frac{[B]^b}{[A]^a}\right)$ for the reaction $aA \leftrightarrow bB$. Redox potentials were calculated by the formula $E_{cell} = \frac{-\Delta G_{rxn}}{n} + E_{SHE}$, where E_{SHE} is the mean experimental value of −4.11 V for the absolute value of the SHE as determined by Williams and co-workers.[45] For possible proton-coupled reduction steps, ΔG_{rxn} was obtained with Hess' law by summing the free energy changes of the separate reduction and protonation steps. To the potential values, −0.59 V is then added to convert to values relative to the Ag/$AgNO_3$ (0.01 M in acetonitrile) reference electrode. We use 1 atm as the standard state for gaseous CO_2 and CO, the pure liquid as the standard state for solvent THF, and 1 M as the standard state for solutes except for Cl^- (0.001 M) and H^+ (10^{-14} M), and we note that such calculations are typically reliable to ±0.30 V.[46]

https://doi.org/10.1021/acs.inorgchem.2c02400
Inorg. Chem. XXXX, XXX, XXX−XXX

Scheme 2. Abridged Square Scheme Calculated for 1 in THF[a]

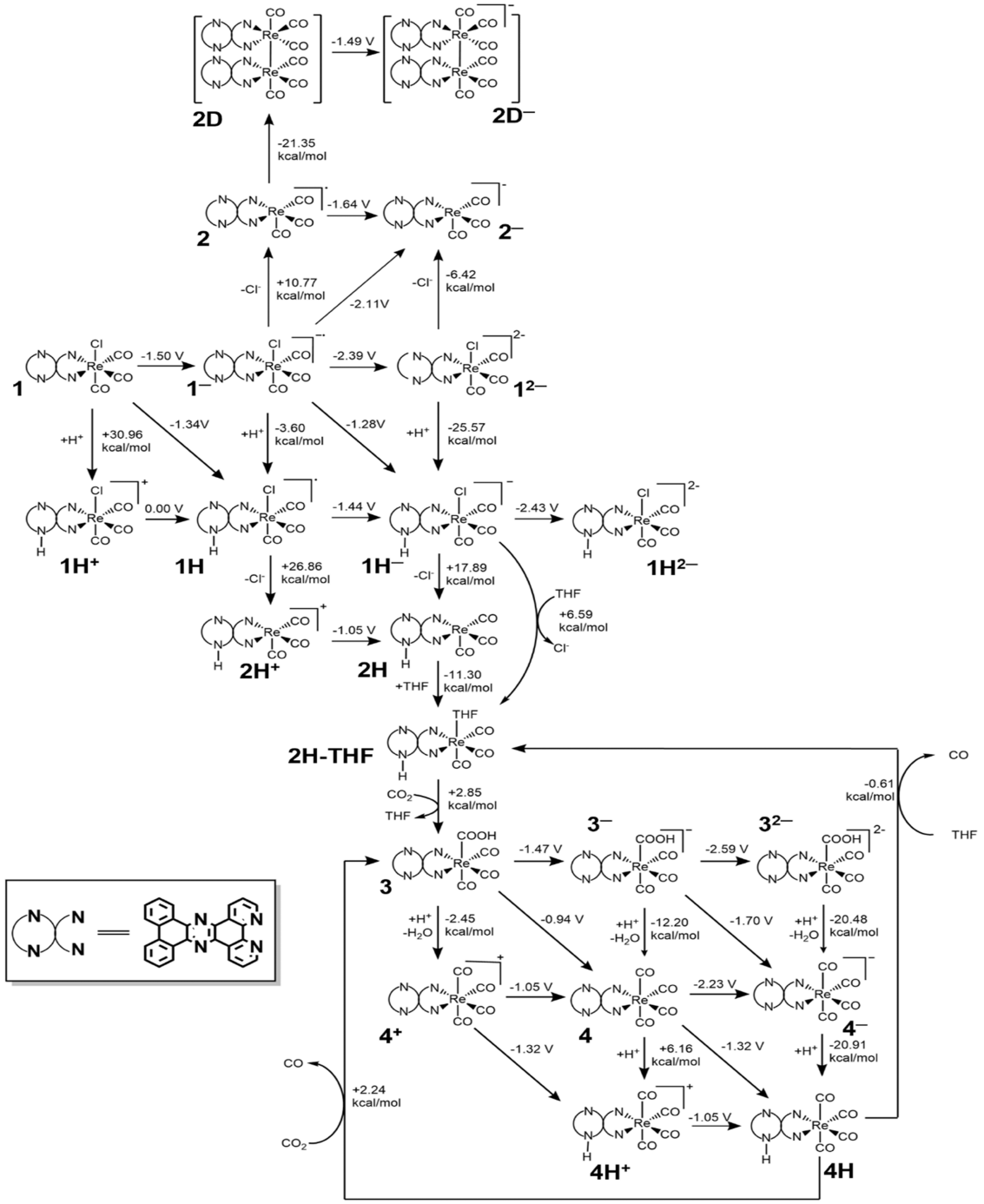

[a]The energetics of the electrochemical processes (horizontal) is shown by the reduction potential vs $Ag/AgNO_3$, and that of the chemical reactions (vertical) is shown by the standard Gibbs free energy change. We use 1 atm as the standard state for gaseous CO_2 and CO, the pure liquid as the standard state for solvent THF, and 1 M as the standard state for solutes except for Cl^- (0.001 M) and H^+ (10^{-14} M). We note that such calculations are typically reliable to ±0.30 V or ±6.9 kcal/mol.

The calculated square scheme is shown in Scheme 2, which is condensed to focus on processes with proton and CO_2 present. In the scheme, the energetics of the electrochemical processes are shown by the equilibrium reduction potentials and that of chemical reactions by the standard Gibbs free energy change (ΔG^0).

According to our calculations, without the involvement of protons, the $\mathbf{1}/\mathbf{1}^-$ equilibrium reduction potential is −1.50 V. Subsequently $\mathbf{1}^-$ can undergo dechlorination, though with considerable energy cost (ΔG^0 = +10.77 kcal/mol, with $[Cl^-]$ = 0.001 M as the standard state). However, dechlorinated species **2** has a strong tendency to dimerize to produce **2D** (ΔG^0 = −21.35 kcal/mol), which may shift the equilibrium to favor the dechlorination of $\mathbf{1}^-$. Further, **2D** can readily undergo an additional one-electron reduction (E^0 = −1.49 V) to produce $\mathbf{2D}^-$, suggesting both **2D** and $\mathbf{2D}^-$ could both be present at the potential applied to produce $\mathbf{1}^-$. At a cathodic potential of −2.11 V, $\mathbf{1}^-$ undergoes a concerted reduction and

https://doi.org/10.1021/acs.inorgchem.2c02400
Inorg. Chem. XXXX, XXX, XXX−XXX

dechlorination to produce $\mathbf{2}^-$, an analogue of the active catalysts for CO_2 binding and reduction in $Re(bpy)(CO)_3Cl$ and derivatives.[14,16,22] Alternatively, $\mathbf{1}^-$ can be reduced to $\mathbf{1}^{2-}$ at a more negative potential (−2.39 V), and $\mathbf{2}^{2-}$ readily undergoes dechlorination to yield $\mathbf{2}^-$ (ΔG^0 = −6.42 kcal/mol, at $[Cl^-]$ = 0.001 M).

Our calculation showed that $\mathbf{1}^-$, due to the pyrazinyl moiety, is a strong Brønsted base, with a conjugated acid having a pK_a of 16.2 in THF. Thus, at pH = 14, **1** may undergo a proton-coupled reduction to form **1H** with an equilibrium reduction potential of −1.34 V, more positive than the $\mathbf{1}/\mathbf{1}^-$ potential. A neutral radical, **1H** can readily undergo another reduction at a slightly more negative of −1.44 V to yield $\mathbf{1H}^-$, which can also undergo dechlorination to yield **2H** with a significant thermodynamic cost (ΔG^0 = +17.89 kcal/mol). Alternatively, $\mathbf{1H}^-$ may undergo chloride substitution by the solvent, leading to **2H-THF**, with ΔG^0 = +6.59 kcal/mol. Here, we assume $[H^+] = 10^{-14}$ M as an estimate, which is the value for 0.10 M phenol dissolved in THF (pK_a = 27.8).[47] This value is chosen because 0.10 M phenol solution leads to a comparable shift in the first reduction peak as the THF/water mixture (5% vol/vol) under the CO_2 atmosphere, where $[H^+]$ is difficult to assess.[48] The uncertainty in $[H^+]$ caused by this comparison does not change our calculated results significantly, since changing the pH value by one unit changes the chemical potential of H^+ by 1.36 kcal/mol (0.059 eV).

With CO_2 present, adduct **3** can form from **2H** with ΔG^0 = −8.45 kcal/mol or from **2H-THF** with ΔG^0 = +2.85 kcal/mol, making the overall conversion of $\mathbf{1H}^-$ to **3** disfavored by ΔG^0 = +9.44 kcal/mol. We note that despite **2H** being *N*-protonated, **3** as the stable form of its CO_2-adduct is *O*-protonated because of stronger Brønsted basicity of Re−COO^-.[49] Meanwhile, **3** can be reduced to $\mathbf{3}^-$ at a potential (E^0 = −1.47 V) close to that for the $\mathbf{1}/\mathbf{1H}$ and the $\mathbf{1H}/\mathbf{1H}^-$ couples (−1.33 and −1.44 V, respectively), suggesting that, with a proton source and CO_2 present, both **3** and $\mathbf{3}^-$ could appear in solution at the potential applied to produce **1H**. This is truly remarkable considering that $\mathbf{3}^-$ is a reduction product from **1** by three electrons. Production of CO and regeneration of the catalyst can proceed through multiple pathways consisting of protonation, reduction, and dehydration that converge on a protonated tetracarbonyl species **4H**. As lower-energy pathways, $\mathbf{3}^-$ can undergo proton-assisted dehydration to yield a tetracarbonyl species **4**, followed by stepwise or concerted protonation and reduction to produce **4H**. Alternatively, $\mathbf{3}^-$ may undergo further reduction concerted with protonation and dehydration at a more negative potential (E^0 = −1.70 V) to produce tetracarbonyl species $\mathbf{4}^-$ and subsequently its conjugated acid **4H**. With assistance of the solvent or CO_2, **4H** can subsequently release CO to regenerate **2H-THF** or **3** with very little energy cost (ΔG^0 = −0.61 and +2.24 kcal/mol, respectively) to complete the catalytic cycle.

The calculated thermodynamics shown in Scheme 2 outlines electrochemical pathways largely consistent with our CV results. By comparing the reduction peaks observed in CV measurements and the calculated values, we can tentatively assign the observed reduction events, though with the caution that the experimentally observed reduction peak positions are not equilibrium potentials. The two reduction events observed in argon can be attributed to the reduction of **1** to $\mathbf{1}^-$ and $\mathbf{1}^-$ to $\mathbf{2}^-$, respectively, the latter accompanied by concerted dechlorination. The observed peak positions (−1.40 and −1.90 V, Figure 1a) within the error of calculations agree quite well with the calculated equilibrium potentials for $\mathbf{1}/\mathbf{1}^-$ (−1.50 V) and $\mathbf{1}^-/\mathbf{2}^-$ (−2.11 V). Such an assignment is consistent with previously reported observations for $Re(bpy)(CO)_3Cl$ and will be investigated further in the future.

In this manuscript, we focus on the electrochemical processes in CO_2 with Brønsted acid added, in which the first observed reduction peak position (−1.30 V) agrees well with the calculated equilibrium potential for the $\mathbf{1}/\mathbf{1H}$ couple (−1.34 V), a proton-coupled reduction process as evidenced by the position shift with added Brønsted acid. The neutral **1H** subsequently undergoes a one-electron reduction to produce $\mathbf{1H}^-$, which has a calculated equilibrium potential close to that of the $\mathbf{1}/\mathbf{1H}$ couple and, in practice, can merge with the $\mathbf{1}/\mathbf{1H}$ reduction to produce the observed doubling of the peak current. The second peak experimentally observed at −1.65 V agrees well with the calculated equilibrium potential (−1.47 V) for the $\mathbf{3}/\mathbf{3}^-$ couple. An irreversible process coupled with a preceding homogeneous chemical reaction (producing **3**), the $\mathbf{3}/\mathbf{3}^-$ reduction is affected by kinetic factors and its experimental peak position may deviate significantly from its equilibrium potential.[50] Subsequent release of CO and regeneration of the catalyst appears to agree with the reduction of $\mathbf{3}^-$ concerted with protonation and dehydration to produce $\mathbf{4}^-$. We speculate that such a proton-coupled reduction process may be favored because the protonation and the reduction both occur at the carboxylic acid moiety (Figure S-8).[51] In contrast, alternative pathways suggested by our calculations, such as $\mathbf{3}^- \rightarrow \mathbf{4} \rightarrow \mathbf{4H}$, may occur at lower rates, which will be further investigated in the future.

Calculations of CO Stretching Frequencies. To verify the proposed pathway outlined in Scheme 2, we calculated the CO stretching frequencies in all of the key intermediates to examine the possibility of identifying them with infrared spectroscopy. The infrared spectroelectrochemistry (IR-SEC) technique has been widely applied to investigate reaction intermediates produced under electrochemical potentials.[22,52] In particular, high sensitivity of the CO stretching frequency to the electronic environment at the metal centers leads to characteristic spectra for chemical species derived from the metal complexes.[19,22,53] For this purpose, we calculated the CO stretching frequency of all of the species in Scheme 2, and the results are listed in Table 1. The vibrational frequencies were calculated in an implicit solvent-corrected potential energy surface, with the conductor-like polarizable continuum model (CPCM) method[34−37] to account for the solvation energy in THF (ε = 7.25).

As detailed in the Supporting Information, to account for the anharmonicity of CO stretching and any systematic error in the frequency calculations, we have employed two error-correction schemes, one additive and the other multiplicative, by fitting experimental values reported for $Re(bpy)(CO)_3Cl$ and its reduction products in THF.[22] In the first scheme (additive), an empirical correction constant of −81 cm^{-1} was obtained, which was then applied to the calculated CO stretching frequencies for all species derived from **1** (shown in Table 1). An alternative approach is to linearly scale the calculated CO stretching values with a multiplicative correction factor (0.96023), which, as shown in the Supporting Information, leads to almost the same values because of the narrow spectral range of the CO stretching frequencies in question. Remarkably, with the same correction, our calculations could reproduce the observed IR frequencies with agreement better than 15 cm^{-1}, mostly within 10 cm^{-1},

https://doi.org/10.1021/acs.inorgchem.2c02400
Inorg. Chem. XXXX, XXX, XXX−XXX

Table 1. Calculated Carbonyl Stretching Frequencies for Species in Scheme 2 and Assignment of Experimental Frequencies[a]

species	calculated (cm^{-1})	experimental (cm^{-1})
1	2016, 1912, 1897	2019, 1915, 1893
$\mathbf{1}^-$	2005, 1896, 1882	2001, *1893*, 1875
$\mathbf{1}^{2-}$	1982, 1865, 1855	
$\mathbf{1H}^+$	2021, 1923, 1906	
1H	2015, 1911, 1895	2013, 1908, 1890
$\mathbf{1H}^-$	2008, 1898, 1883	2001, *1890*, *1876*
2	1996, 1896, 1887	
$\mathbf{2}^-$	1938, 1839, 1835	
2H	2034, 1929, 1915	
2H-THF	2029, 1917,1913	
2D	1991, 1958, 1898, 1878, 1866	
$\mathbf{2D}^-$	1979, 1945, 1886, 1864, 1851	1977, 1940, 1876, 1865, 1842
3	2008, 1906, 1897, (1621)	2001, *1908*, *1890*, (1620 br.)
$\mathbf{3}^-$	1998, 1892, 1881, (1630)	1998, 1883, 1870, (1620 br.)
4+	2124, 2014, 2008, 1967	
4	2108, 1994, 1980, 1938	
$\mathbf{4}^-$	2099, 1982, 1960, 1916	

[a]The calculated values were obtained after the correction described in the text. In parentheses are calculated C═O stretching frequencies, and in italic are peaks that are anticipated from the calculations yet cannot be identified with high certainty due to overlap with those of other species.

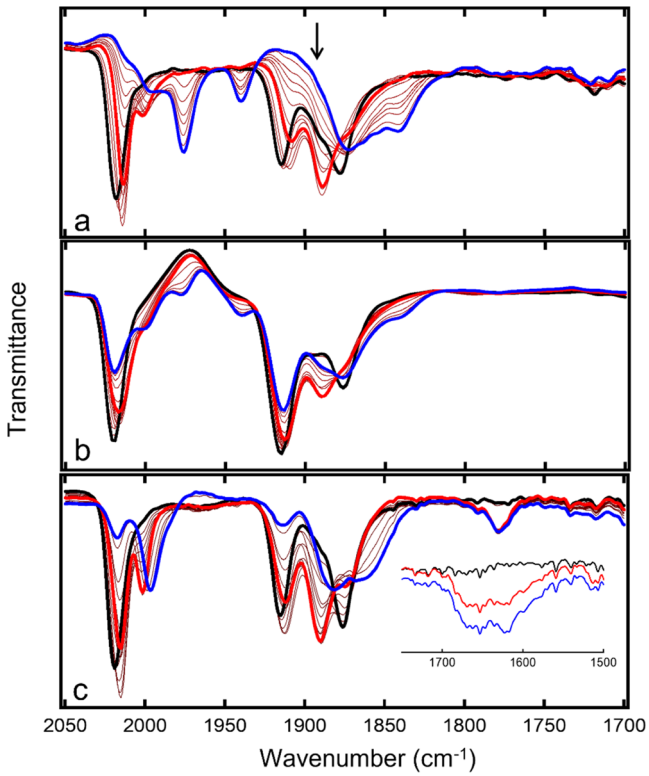

Figure 2. IR-SEC spectra of **1** in dry THF in (a) argon, (b) argon with phenol, and (c) CO_2 and D_2O. The potential was increasingly more negative in the order of black, red, and blue curves. Marked by the arrow in (a) at 1893 cm^{-1} is the peak belonging to monomeric **1**. In the inset in (c) are the spectra between 1500 and 1750 cm^{-1}, and the peak at 1780 cm^{-1} is residual solvent peak.

giving us great confidence in assigning the species based on our calculations. The same correction was applied to C═O stretching frequencies (in parentheses in the left column in Table 1) as well for Re−COOH species (**3** and $\mathbf{3}^-$).

IR Spectroelectrochemistry Studies. We applied infrared spectroelectrochemistry (IR-SEC) to investigate the reaction intermediates that formed when **1** (Figure 2) undergoes sequential reduction processes without and with proton present, respectively. As described in the experimental details (Supporting Information), the IR spectroelectrochemistry (IR-SEC) studies were conducted with an air-tight, transmission-mode thin-layer electrochemical (OTTLE) cell equipped with a pair of CaF_2 windows.[54] In the cell the working electrode is made of a Pt wire mesh (200 wires/cm). Another Pt wire mesh (32 wires/cm) is used as the counter electrode and an Ag wire (0.05 mm diameter) as a pseudo-reference electrode. The reference electrode is placed ∼0.5 mm away from an edge of the working electrode mesh. The cell was mostly masked so that the incident IR beam can only go through the working electrode mesh. Solvent and supporting electrolyte are the same as those used for the CV measurements, and all solutions were prepared and loaded to the cell under dry nitrogen in a glovebox. The IR spectra were recorded with an FTIR spectrometer with a spectral resolution of 2.0 cm^{-1}. In the experiments, the potential was scanned with a step size of −50 mV and held for 30 min for multiple spectra to be measured. As a result of the slow scan in the potential, the experiments can provide spectroscopic signature for processes occurring near the electrodes or in the solution at a much slower rate than those in the time scale of the CV measurements.

Figure 2 shows the evolution of IR spectra obtained over a range of 400 mV, starting from an initial potential that was negative enough to produce spectral changes observable over a 30 min period. In the direction of increasingly negative potential, the spectra are represented with black curves changing to red then to blue, with the spectra in-between represented with thin brown curves. In all three panels (under (a) argon, (b) argon with phenol, (c) CO_2 with D_2O), the black curves belong to the starting material **1**, in which three major peaks (2019, 1915, 1876 cm^{-1}) are observed together with a shoulder at 1893 cm^{-1} (marked by the black arrow in Figure 2a). Concentration-dependent IR measurements (Figure S-9) showed that the 2019, 1915, and 1893 cm^{-1} peaks are due to monomeric **1** ($A'(1)$, $A'(2)$, and A'' normal modes, respectively), which have excellent agreement with calculated values (Table 1), and that the peak at 1876 cm^{-1} is due to aggregates of **1** in the solution. Under the argon atmosphere (Figure 2a), when reduction starts to occur, major peaks at 2013, 1908, and 1890 cm^{-1} develop with two minor ones at 2001 and 1875 cm^{-1}, respectively (red curve). Under a more negative potential, two strong peaks appear at 1977 and 1940 cm^{-1}, with a broad feature between 1876 and 1842 cm^{-1}. Comparison with calculated results in Table 1 shows that the 2013, 1908, and 1890 cm^{-1} peaks agree remarkably well with the calculated values for **1H**, and the 2001 and the 1875 cm^{-1} peaks agree with $\mathbf{1}^-$. The presence of the protonated **1H** even when no water was intentionally added can be attributed to residual water in the solution or extraction of proton from the electrolyte $TBAPF_6$,[55] which is often encountered.[56] The peaks at 1977, 1940, 1876, and 1842 cm^{-1} can be assigned to the dimeric $\mathbf{2D}^-$, showing that **1** upon the one-electron reduction can slowly release the chloride, similar to $Re(bpy)(CO)_3Cl$.[57] Presence of $\mathbf{2D}^-$ is consistent with Scheme 2, which shows that

https://doi.org/10.1021/acs.inorgchem.2c02400
Inorg. Chem. XXXX, XXX, XXX−XXX

1^- can readily dimerize and the dimer **2D** can be further reduced to produce $2D^-$ at the potential applied to produce 1^-.

With phenol as a Brønsted acid under argon (Figure 2b), when reduction occurs, the spectrum is dominated by **1H** (red curve). Under a more negative potential (blue curve) dimeric $2D^-$ was observed though in a much smaller amount. This agrees with Scheme 2, which shows dechlorination and the subsequent dimerization of **1H** is thermodynamically less favored. Meanwhile, a minor peak appears at 2001 cm^{-1}, which agrees well with the calculated $A'(1)$ mode in either 1^- or $1H^-$ (Table 1). However, based on its intensity relative to those of $2D^-$ in the spectra, we believe that $1H^-$ is the major species responsible because of the strong tendency of 1^- to protonate and to form dimeric species over the comparable time duration. The two lower-frequency modes of $1H^-$, expected at 1898 and 1883 cm^{-1}, respectively, overlap with peaks in **1H** and $2D^-$. This is consistent with our calculations that, under the applied potential, **1H** can be readily reduced to $1H^-$, and with the peak current doubling in our CV measurements.

Under a CO_2 atmosphere with D_2O added as a Brønsted acid (Figure 2c), when reduction occurs an intense peak at 2001 cm^{-1} appears besides those assigned to **1H**. Meanwhile, the peak at 1890 cm^{-1} that belongs to **1H** grows in intensity, indicating contribution from an additional species. Even though our calculation showed 1^-, $1H^-$, and **3** (Table 1) all have peaks near 2001 and 1890 cm^{-1}, we believe it is the most reasonable under the reaction condition to assign them to **3**. The 2001 cm^{-1} peak here has much a higher intensity than that in Figure 2a or Figure 2b, indicating the high stability of the species under these conditions. And dimeric $2D^-$ would have been expected in equilibrium with 1^- or $1H^-$ but is not present. Further, this is consistent with the broad peak appearing at 1620 and 1660 cm^{-1}, respectively (inset in Figure 2c) that indicates covalent binding of CO_2 and formation of metallocarboxylic species. Compound **3** may form through **2H** reacting with CO_2, or directly from $1H^-$ through substitution of the chloride by CO_2, in both cases followed by protonation of the Re−COO^- and deprotonation of the pyrazinyl nitrogen. At a more negative potential (blue curve) appears a peak at 1998 cm^{-1} with two broad ones at 1883 and 1870 cm^{-1}, respectively. By comparing with our calculated results, they can be assigned to 3^-, which forms from **3** because the applied potential is approaching the equilibrium potential for $3/3^-$. Further decreasing the applied potential only leads to broadening of the peaks assigned to 3^- with no tetracarbonyl or other species observed, presumably because of their high reactivity under the experimental conditions.

With the IR peaks assigned, our IR-SEC measurements largely confirm the calculated electrochemical pathway outlined in Scheme 2. Key species **1H**, $1H^-$, **3**, and 3^- have been identified spectroscopically, outlining a previously unknown, lower-energy reaction pathway that decreases CO_2 reduction overpotential. Remarkably, to our best knowledge, it is the first time that rhenium−carboxylic acid (Re−COOH) species **3** and 3^- were observed in the presence of proton and CO_2 under an applied potential, though a dimethyl bipyridyl analogue of **3** was previously synthesized and isolated.[58]

Roles of Pyrazinyl Nitrogen. Our work reveals that, due to the pyrazinyl moiety in the diimine ligand, the CO_2 activation pathway by **1** is drastically different from that generally accepted for Re(bpy)$(CO)_3$Cl. Figure 3 summarizes the proton-coupled pathway revealed in this work (orange lines), showing the Gibbs free energy change of each step at an applied potential that is equal to the equilibrium potential for the **1**/**1H** couple (−1.33 V). For comparison, a hypothetical, unprotonated pathway from **1** is also shown based on the pathway for Re(bpy)$(CO)_3$Cl (Figure 3, blue lines), in which proton is not involved until the last steps.[57] In the figure represented with the dashed lines are high-energy intermediates that are bypassed through other, lower-energy pathways, i.e., 2H, the dechlorinated product of $1H^-$, bypassed by solvent-assisted dechlorination (via **2H-THF**), and 1^{2-} by concerted reduction-dechlorination. At each step, the proton-coupled pathway is lower in energy by 2.303 $RT(pK_a - pH)$, where pK_a is for the conjugated acid of the intermediates. Clearly, in the unprotonated pathway, producing 2^- through concerted reduction-dechlorination requires the most negative electrochemical potential and determines the CO_2 reduction overpotential.[57] In contrast, in the proton-coupled pathway, it is the formation of 4^- through which catalyst regeneration occurs, that requires the most negative potential. For the initial catalyst activation, proton-coupled first reduction makes the second reduction occur much more readily (−1.44 V vs −2.11 V). Though requiring more negative potential to regenerate the catalyst, the proton-coupled pathway overall leads to a lower CO_2 reduction overpotential. We note that *N*-protonation in reduced metal complexes with polypyridyl ligands that contain additional noncoordinating pyrazinyl or pyrimidinyl moieties has been previously investigated.[59−62] In those cases, the protonation modifies the electronic structures of the complexes yet not to the extent of altering catalytic pathways like in the case of **1**.

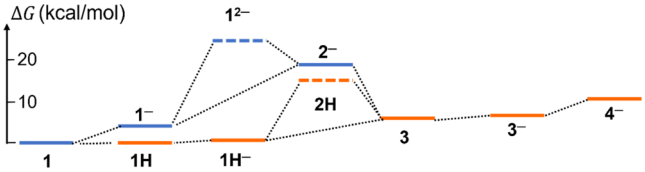

Figure 3. Comparison between the calculated energetics of the proton-coupled (orange lines) and unprotonated (blue lines) pathways for CO_2 activation at the equilibrium potential to produce **1H** (−1.33 V).

The importance of the protonation at pyrazinyl nitrogen in the proton-coupled pathway makes the conjugation size of the diamine ligand an important parameter for the CO_2 reduction. Nitrogen atoms in the one-electron reduced catalyst adopt the sp^3-configuration, and the basicity is greatly affected by delocalization of the nitrogen lone electron pair over the aromatic framework. Increasing the conjugation size in the arylamines lowers the energy of delocalized electronic levels, shifting electron density to the conjugated system and decreasing the electron density and hence the basicity of the pyrazinyl nitrogen. Such a trend has been experimentally demonstrated in the basicity of small molecular arylamines. For example, pK_a for the conjugate acid of aniline in water is 4.62, for 1-naphthylamine is 3.92,[63] and for amino-pyrene is 3.6.[64] Thus, for Re complexes with diamine ligands of increasing size, the energetic advantage of the proton-coupled pathway over the unprotonated one will decrease.

The lower energy of delocalized electronic levels that decreases basicity at the pyrazinyl nitrogen atoms will also decrease the electron density at the coordinating nitrogen in the diimine ligand, impacting the activation of the catalyst and the subsequent catalytic cycle. Such an effect was previously

https://doi.org/10.1021/acs.inorgchem.2c02400
Inorg. Chem. XXXX, XXX, XXX−XXX

reported with Re(diimine)$(CO)_3$Cl complexes that the electron density transferred to the coordinating nitrogen atoms upon electrochemical reduction is crucial to the labilization of the halide.[65] Thus, a diimine ligand with a larger conjugation size will make the dechlorination more difficult for the catalyst activation. Meanwhile, the decreased electron density at the coordinating nitrogen decreases the nucleophilicity of the Re center after the dechlorination, hindering the binding of CO_2 and its subsequent reduction to CO. This agrees with the sufficient stability of $\mathbf{1H}^-$, **3**, and $\mathbf{3}^-$ for the spectroscopic detection in our studies, as well as the turnover frequency of **1** being nearly an order of magnitude lower than Re(bpy)$(CO)_3$Cl.[56]

Heterogenization of the Re(bpy)$(CO)_3$Cl with a pyrazinyl linkage (**A** in Scheme 1) can be considered as an analogue of **1** in an extreme case with a graphene of infinite size, and we can speculate the roles of the pyrazinyl nitrogen in the catalysis based on the insights obtained with **1**. Because of the tendency of electron delocalization, with one electron added to the system basicity of the pyrazinyl nitrogen is expected to be too low to direct the catalysis along the proton-coupled pathway. Meanwhile, the electron delocalization decreases the electron density at the coordinating nitrogen in the diimine ligand, impacting the activation of the catalyst and the subsequent catalytic cycle. Adding more electrons to the system can overcome such effects. The spilling of electron density from the graphene to the pyrazinyl nitrogen can turn on the proton-coupled pathway, though requiring a more negative potential that may not be significantly different from that needed for Re(bpy)$(CO)_3$Cl.

CONCLUSIONS

Here, we show a conjugated pyrazinyl moiety in the diamine ligand for the *fac*-Re(α-diimine)$(CO)_3$Cl complexes opens a proton-coupled, lower-energy pathway for electrocatalytic CO_2 reduction. Proton-coupled first reduction of complex **1** yields a neutral radical species and makes the second reduction occur much more easily. As a result, CO_2 is selectively reduced to CO at a lower overpotential. Because the pathways hinge on the basicity of the pyrazinyl nitrogen, we propose it as a factor that imposes a constraint on the conjugation size of the ligand for the pathway to be effective. Increasing the size of the ligand will also decrease the electron density in the diimine that chelates to the metal center, making catalyst activation more difficult and decreasing the catalytic reaction rate. Our results provide important insights regarding electronic coupling between graphitic carbon electrodes with covalently immobilized molecular catalysts. In addition, we believe the proton-coupled reduction introduced by the pyrazinyl moiety is a general approach to lower reduction overpotential for other catalytic systems, and work is ongoing to test this hypothesis.

ASSOCIATED CONTENT

Supporting Information

The Supporting Information is available free of charge at https://pubs.acs.org/doi/10.1021/acs.inorgchem.2c02400.

Details of experiments and calculations, catalyst synthesis and characterization (^{1}H NMR and FTIR), detailed electrochemical studies including bulk electrolysis for determination of faradic efficiency and reaction rate, GC analysis of product, calculated IR frequencies, and calculated atomic coordinates of relevant species (PDF)

AUTHOR INFORMATION

Corresponding Authors

Krishnan Raghavachari − *Department of Chemistry, Indiana University, Bloomington, Indiana 47405, United States;* orcid.org/0000-0003-3275-1426; Email: kraghava@indiana.edu

Liang-shi Li − *Department of Chemistry, Indiana University, Bloomington, Indiana 47405, United States;* orcid.org/0000-0001-7566-8492; Email: li23@indiana.edu

Authors

Sruthy K. Chandy − *Department of Chemistry, Indiana University, Bloomington, Indiana 47405, United States;* orcid.org/0000-0002-1061-647X

Scott A. Bowers − *Department of Chemistry, Indiana University, Bloomington, Indiana 47405, United States;* orcid.org/0000-0001-7044-6719

Minyang Yin − *Department of Chemistry, Indiana University, Bloomington, Indiana 47405, United States*

Lu Liu − *Department of Chemistry, Indiana University, Bloomington, Indiana 47405, United States*

Complete contact information is available at: https://pubs.acs.org/10.1021/acs.inorgchem.2c02400

Author Contributions

†S.K.C. and S.A.B. contributed equally to the work.

Notes

The authors declare no competing financial interest.

ACKNOWLEDGMENTS

The authors acknowledge the financial support of the National Science Foundation Grant CHE-1764264. The Big Red 3 Supercomputing facility at Indiana University was used for most of the calculations in this study. The authors thank James Clark and Dr. Norman Dean in their department for assistance with the gas chromatography analysis.

REFERENCES

(1) Nørskov, J. K.; Bligaard, T.; Logadottir, A.; Bahn, S.; Hansen, L. B.; Bollinger, M.; Bengaard, H.; Hammer, B.; Sljivancanin, Z.; Mavrikakis, M.; Xu, Y.; Dahl, S.; Jacobsen, C. J. H. Universality in Heterogeneous Catalysis. *J. Catal.* **2002**, *209*, 275−278.

(2) Appel, A. M.; Bercaw, J. E.; Bocarsly, A. B.; Dobbek, H.; DuBois, D. L.; Dupuis, M.; Ferry, J. G.; Fujita, E.; Hille, R.; Kenis, P. J.; Kerfeld, C. A.; Morris, R. H.; Peden, C. H. F.; Portis, A. R.; Ragsdale, S. W.; Rauchfuss, T. B.; Reek, J. N. H.; Seefeldt, L. C.; Thauer, R. K.; Waldrop, G. L. Frontiers, Opportunities, and Challenges in Biochemical and Chemical Catalysis of CO_2 Fixation. *Chem. Rev.* **2013**, *113*, 6621−6658.

(3) Rosca, V.; Duca, M.; de Groot, M. T.; Koper, M. T. M. Nitrogen Cycle Electrocatalysis. *Chem. Rev.* **2009**, *109*, 2209−2244.

(4) Zhang, W.; Lai, W.; Cao, R. Energy-Related Small Molecule Activation Reactions: Oxygen Reduction and Hydrogen and Oxygen Evolution Reactions Catalyzed by Porphyrin- and Corrole-Based Systems. *Chem. Rev.* **2017**, *117*, 3717−3797.

(5) Lyaskovskyy, V.; de Bruin, B. Redox Non-Innocent Ligands: Versatile New Tools to Control Catalytic Reactions. *ACS Catal.* **2012**, *2*, 270−279.

(6) Luca, O. R.; Crabtree, R. H. Redox-Active Ligands in Catalysis. *Chem. Soc. Rev.* **2013**, *42*, 1440−1459.

(7) Zhanaidarova, A.; Jones, S. C.; Despagnet-Ayoub, E.; Pimentel, B. R.; Kubiak, K. P. Re(tBu-bpy)$(CO)_3$Cl Supported on Multi-Walled Carbon Nanotubes Selectively Reduces CO_2 in Water. *J. Am. Chem. Soc.* **2019**, *141*, 17270−17277.
(8) Zhang, S.; Fan, Q.; Xia, R.; Meyer, T. J. CO_2 Reduction: From Homogeneous to Heterogeneous Electrocatalysis. *Acc. Chem. Res.* **2020**, *53*, 255−264.
(9) Jackson, M. N.; Oh, S.; Kaminsky, C. J.; Chu, S. B.; Zhang, G.; Miller, J. T.; Surendranath, Y. Strong Electronic Coupling of Molecular Sites to Graphitic Electrodes via Pyrazine Conjugation. *J. Am. Chem. Soc.* **2018**, *140*, 1004−1010.
(10) Oh, S.; Gallagher, J. R.; Miller, J. T.; Surendranath, Y. Graphite-Conjugated Rhenium Catalysts for Carbon Dioxide Reduction. *J. Am. Chem. Soc.* **2016**, *138*, 1820−1823.
(11) Jackson, M. N.; Surendranath, Y. Molecular Control of Heterogeneous Electrocatalysis through Graphite Conjugation. *Acc. Chem. Res.* **2019**, *52*, 3432−3441.
(12) Hawecker, J.; Lehn, J.-M.; Ziessel, R. Electrocatalytic Reduction of Carbon Dioxide Mediated by Re(bipy)$(CO)_3$Cl (bipy = 2,2′-bipyridine). *J. Chem. Soc., Chem. Commun.* **1984**, 328−330.
(13) Hawecker, J.; Lehn, J.-M.; Ziessel, R. Photochemical and Electrochemical Reduction of Carbon Dioxide to Carbon Monoxide Mediated by (2,2′-Bipyridine)tricarbonylchlororhenium(I) and Related Complexes as Homogeneous Catalysts. *Helv. Chim. Acta* **1986**, *69*, 1990−2011.
(14) Sullivan, B. P.; Bolinger, C. M.; Conrad, D.; Vining, W. J.; Meyer, T. J. One- and Two-Electron Pathways in the Electrocatalytic Reduction of CO_2 by *fac*-Re(bpy)$(CO)_3$Cl (bpy = 2,2'-bipyridine). *J. Chem. Soc., Chem. Commun.* **1985**, 1414−1416.
(15) Morris, A. J.; Meyer, G. J.; Fujita, E. Molecular Approaches to the Photocatalytic Reduction of Carbon Dioxide for Solar Fuels. *Acc. Chem. Res.* **2009**, *42*, 1983−1994.
(16) Grice, K. A.; Kubiak, C. P. Recent Studies of Rhenium and Manganese Bipyridine Carbonyl Catalysts for the Electrochemical Reduction of CO_2. *Adv. Inorg. Chem.* **2014**, *66*, 163−188.
(17) Qiao, X.; Li, Q.; Schaugaard, R. N.; Noffke, B. W.; Liu, Y.; Li, D.; Liu, L.; Raghavachari, K.; Li, L.-s. Well-Defined Nanographene−Rhenium Complex as an Efficient Electrocatalyst and Photocatalyst for Selective CO_2 Reduction. *J. Am. Chem. Soc.* **2017**, *139*, 3934−3937.
(18) Bodige, S.; MacDonnell, F. M. Synthesis of free and ruthenium coordinated 5,6-diamino-1,10-phenanthroline. *Tetrahedron Lett.* **1997**, *38*, 8159−8160.
(19) Stor, G. J.; Hartl, F.; van Outersterp, J. W. M.; Stufkens, D. J. Spectroelectrochemical (IR, UV/Vis) Determination of the Reduction Pathways for a Series of [Re$(CO)_3$(α-diimine)L'] (L' = Halide, Otf^-, THF, MeCN, n-PrCN, PPh_3, $P(OMe)_3$) Complexes. *Organometallics* **1995**, *14*, 1115−1131.
(20) Costentin, C.; Savéant, J.-M. Multielectron, Multistep Molecular Catalysis of Electrochemical Reactions: Benchmarking of Homogeneous Catalysts. *ChemElectroChem* **2014**, *1*, 1226−1236.
(21) Costentin, C.; Drouet, S.; Robert, M.; Savéant, J.-M. Turnover Numbers, Turnover Frequencies, and Overpotential in Molecular Catalysis of Electrochemical Reactions. Cyclic Voltammetry and Preparative-Scale Electrolysis. *J. Am. Chem. Soc.* **2012**, *134*, 11235−11242.
(22) Johnson, F. P.; George, M. W.; Hartl, F.; Turner, J. J. Electrocatalytic Reduction of CO_2 Using the Complexes [Re(bpy)-$(CO)_3L]^n$ (n = +1, L = $P(OEt)_3$, CH_3CN; n = 0,L = Cl^-, Otf^-; bpy= 2,2'-Bipyridine; Otf^- = CF_3SO_3) as Catalyst Precursors: Infrared Spectroelectrochemical Investigation. *Organometallics* **1996**, *15*, 3374−3387.
(23) Hayashi, Y.; Kita, S.; Brunschwig, B. S.; Fujita, E. Involvement of a Binuclear Species with the Re-C(O)O-Re Moiety in CO_2 Reduction Catalyzed by Tricarbonyl Rhenium(I) Complexes with Diimine Ligands: Strikingly Slow Formation of the Re-Re and Re-C(O)O-Re Species from Re(dmb)(CO)3S (dmb = 4,4'-Dimethyl-2,2'-bipyridine, S = Solvent). *J. Am. Chem. Soc.* **2003**, *125*, 11976−11987.
(24) Li, Q.; Noffke, B.; Wang, Y.; Menezes, B.; Peters, D. G.; Raghavachari, K.; Li, L.-S. Electrocatalytic Oxygen Activation by Carbanion Intermediates of Nitrogen-Doped Graphitic Carbon. *J. Am. Chem. Soc.* **2014**, *136*, 3358−3361.
(25) Frisch, M. J.; Trucks, G. W.; Schlegel, H. B.; Scuseria, G. E.; Robb, M. A.; Cheeseman, J. R.; Scalmani, G.; Barone, V.; Petersson, G. A.; Nakatsuji, H.; Li, X.; Caricato, M.; Marenich, A. V.; Bloino, J.; Janesko, B. G.; Gomperts, R.; Mennucci, B.; Hratchian, H. P.; Ortiz, J. V.; Izmaylov, A. F.; Sonnenberg, J. L.; Williams, A.; Ding, F.; Lipparini, F.; Egidi, F.; Goings, J.; Peng, B.; Petrone, A.; Henderson, T.; Ranasinghe, D.; Zakrzewski, V. G.; Gao, J.; Rega, N.; Zheng, G.; Liang, W.; Hada, M.; Ehara, M.; Toyota, K.; Fukuda, R.; Hasegawa, J.; Ishida, M.; Nakajima, T.; Honda, Y.; Kitao, O.; Nakai, H.; Vreven, T.; Throssell, K.; Montgomery, J. A., Jr.; Peralta, J. E.; Ogliaro, F.; Bearpark, M. J.; Heyd, J. J.; Brothers, E. N.; Kudin, K. N.; Staroverov, V. N.; Keith, T. A.; Kobayashi, R.; Normand, J.; Raghavachari, K.; Rendell, A. P.; Burant, J. C.; Iyengar, S. S.; Tomasi, J.; Cossi, M.; Millam, J. M.; Klene, M.; Adamo, C.; Cammi, R.; Ochterski, J. W.; Martin, R. L.; Morokuma, K.; Farkas, O.; Foresman, J. B.; Fox, D. J.*Gaussian 16*, revision C.01; Gaussian Inc.: Wallingford, CT, 2016.
(26) Vosko, S. H.; Wilk, L.; Nusair, M. Accurate Spin-Dependent Electron Liquid Correlation Energies for Local Spin Density Calculations: a Critical Analysis. *Can. J. Phys.* **1980**, *58*, 1200−1211.
(27) Lee, C.; Yang, W.; Parr, R. G. Development of the Colle-Salvetti Correlation-Energy Formula into a Functional of the Electron Density. *Phys. Rev. B* **1988**, *37*, 785−789.
(28) Becke, A. D. Density-Functional Exchange-Energy Approximation with Correct Asymptotic Behavior. *Phys. Rev. A* **1988**, *38*, 3098−3100.
(29) Becke, A. D. A New Mixing of Hartree−Fock and Local Density-Functional Theories. *J. Chem. Phys.* **1993**, *98*, 1372−1377.
(30) Grimme, S.; Antony, J.; Ehrlich, S.; Krieg, H. A Consistent and Accurate Ab Initio Parametrization of Density Functional Dispersion Correction (DFT-D) for the 94 Elements H-Pu. *J. Chem. Phys.* **2010**, *132*, No. 154104.
(31) Johnson, E. R.; Becke, A. D. A Post-Hartree−Fock Model of Intermolecular Interactions. *J. Chem. Phys.* **2005**, *123*, No. 024101.
(32) Becke, A. D.; Johnson, E. R. A Density-Functional Model of the Dispersion Interaction. *J. Chem. Phys.* **2005**, *123*, No. 154101.
(33) Johnson, E. R.; Becke, A. D. A post-Hartree-Fock Model of Intermolecular Interactions: Inclusion of Higher-Order Corrections. *J. Chem. Phys.* **2006**, *124*, No. 174104.
(34) Klamt, A.; Schüürmann, G. COSMO: A New Approach to Dielectric Screening in Solvents with Explicit Expressions For the Screening Energy and Its Gradient. *J. Chem. Soc., Perkin Trans. 2* **1993**, 799−805.
(35) Andzelm, J.; Kölmel, C.; Klamt, A. Incorporation of Solvent Effects into Density Functional Calculations of Molecular Energies and Geometries. *J. Chem. Phys.* **1995**, *103*, 9312−9320.
(36) Barone, V.; Cossi, M. Quantum Calculation of Molecular Energies and Energy Gradients in Solution by a Conductor Solvent Model. *J. Phys. Chem. A* **1998**, *102*, 1995−2001.
(37) Cossi, M.; Rega, N.; Scalmani, G.; Barone, V. Energies, Structures, and Electronic Properties of Molecules in Solution with the C-PCM Solvation Model. *J. Comput. Chem.* **2003**, *24*, 669−681.
(38) Schäfer, A.; Horn, H.; Ahlrichs, R. Fully Optimized Contracted Gaussian Basis Sets for Atoms Li to Kr. *J. Chem. Phys.* **1992**, *97*, 2571−2577.
(39) Andrae, D.; Häußermann, U.; Dolg, M.; Stoll, H.; Preuß, H. Energy-Adjusted Ab Initio Pseudopotentials for the Second and Third Row Transition Elements: Molecular Test for M2 (M = Ag, Au) and MH (M = Ru, Os). *Theor. Chim. Acta* **1991**, *78*, 247−266.
(40) Schäfer, A.; Huber, C.; Ahlrichs, R. Fully Optimized Contracted Gaussian Basis Sets of Triple Zeta Valence Quality for Atoms Li to Kr. *J. Chem. Phys.* **1994**, *100*, 5829−5835.
(41) Weigend, F.; Ahlrichs, R. Balanced Basis Sets of Split Valence, Triple Zeta Valence and Quadruple Zeta Valence Quality for H to Rn: Design and Assessment of Accuracy. *Phys. Chem. Chem. Phys.* **2005**, *7*, 3297−3305.

https://doi.org/10.1021/acs.inorgchem.2c02400
Inorg. Chem. XXXX, XXX, XXX−XXX

(42) Papajak, E.; Leverentz, H. R.; Zheng, J.; Truhlar, D. G. Efficient Diffuse Basis Sets: cc-pVxZ+ and maug-cc-pVxZ. *J. Chem. Theory Comput.* **2009**, *5*, 1197−1202.
(43) Papajak, E.; Truhlar, D. G. Efficient Diffuse Basis Sets for Density Functional Theory. *J. Chem. Theory Comput.* **2010**, *6*, 597−601.
(44) McQuarrie, D. A.*Statistical Mechanics*; University Science Books, Sausalito, California: 2000.
(45) Donald, W. A.; Leib, R. D.; Demireva, M.; O'Brien, J. T.; Prell, J. S.; Williams, E. R. Directly Relating Reduction Energies of Gaseous $Eu(H2O)_n^{3+}$, n = 55−140, to Aqueous Solution: The Absolute SHE Potential and Real Proton Solvation Energy. *J. Am. Chem. Soc.* **2009**, *131*, 13328−13337.
(46) Noffke, B. W.; Li, Q.; Raghavachari, K.; Li, L.-S. A Model for the pH-Dependent Selectivity of the Oxygen Reduction Reaction Electrocatalyzed by N-Doped Graphitic Carbon. *J. Am. Chem. Soc.* **2016**, *138*, 13923−13929.
(47) Ding, F.; Smith, J. M.; Wang, H. First-Principles Calculation of pKa Values for Organic Acids in Nonaqueous Solution. *J. Org. Chem.* **2009**, *74*, 2679−2691.
(48) Sampaio, R. N.; DiMarco, B. N.; Concepcion, J. J. Proton-Coupled Group Transfer Enables Concerted Protonation Pathways Relevant to Small-Molecule Activation. *Inorg. Chem.* **2021**, *60*, 16953−16965.
(49) Keith, J. A.; Grice, K. A.; Kubiak, C. P.; Carter, E. A. Elucidation of the Selectivity of Proton-Dependent Electrocatalytic CO_2 Reduction by fac-$Re(bpy)(CO)_3Cl$. *J. Am. Chem. Soc.* **2013**, *135*, 15823−15829.
(50) Bard, A. J.; Faulkner, L. R.*Electrochemical Methods Fundamentals and Applications*; Wiley & Sons: Hoboken, 2001.
(51) Darcy, J. W.; Koronkiewicz, B.; Parada, G. A.; Mayer, J. M. A Continuum of Proton-Coupled Electron Transfer Reactivity. *Acc. Chem. Res.* **2018**, *51*, 2391−2399.
(52) Christensen, P.; Hamnett, A.; Muir, A. V. G.; Timney, J. A. An *In Situ* Infrared Study of CO_2 Reduction Catalysed by Rhenium Tricarbonyl Bipyridyl Derivatives. *J. Chem. Soc., Dalton Trans.* **1992**, 1455−1463.
(53) Machan, C. W.; Sampson, M. D.; Chabolla, S. A.; Dang, T.; Kubiak, C. P. Developing a Mechanistic Understanding of Molecular Electrocatalysts for CO_2 Reduction using Infrared Spectroelectrochemistry. *Organometallics* **2014**, *33*, 4550−4559.
(54) Krejčik, M.; Danek, M.; Hartl, F. Simple Construction of an Infrared Optically Transparent Thin-Layer Electrochemical Cell. *J. Electroanal. Chem. Interfacial Electrochem.* **1991**, *317*, 179−187.
(55) Bolinger, C. M.; Sullivan, B. P.; Conrad, D.; Gilbert, J. A.; Story, N.; Meyer, T. J. Electrocatalytic Reduction of CO_2 based on Polypyridyl Complexes of Rhodium and Ruthenium. *J. Chem. Soc., Chem. Commun.* **1985**, 796−797.
(56) Clark, M. L.; Cheung, P. L.; Lessio, M.; Carter, E. A.; Kubiak, C. P. Kinetic and Mechanistic Effects of Bipyridine (bpy) Substituent, Labile Ligand, and Brønsted Acid on Electrocatalytic CO_2 Reduction by Re(bpy) Complexes. *ACS Catal.* **2018**, *8*, 2021−2029.
(57) Riplinger, C.; Sampson, M. D.; Ritzmann, A. M.; Kubiak, C. P.; Carter, E. A. Mechanistic Contrasts between Manganese and Rhenium Bipyridine Electrocatalysts for the Reduction of Carbon Dioxide. *J. Am. Chem. Soc.* **2014**, *136*, 16285−16298.
(58) Gibson, D. H.; Yin, X. Synthesis and Reactions of *fac*-$Re(dmbpy)(CO)_3X$ (dmbpy = 4,4'-dimethyl-2,2'-bipyridyl; X= COOH, COOMe, H, OH, and OCHO). *J. Am. Chem. Soc.* **1998**, *120*, 11200−11201.
(59) D'Angelantonio, M.; Mulazzani, Q. G.; Venturi, M.; Ciano, M.; Hoffman, M. Z. One-Electron Reduction of Ruthenium(II)-Diimine Complexes: Characterization of Reduced Species Containing 2,2'-Bipyridine, 2,2'-Bipyrimidine, and 2,2'-Bipyrazine in Aqueous Solution. *J. Phys. Chem. A* **1991**, *95*, 5121−5129.
(60) Casalboni, F.; Mulazzani, Q. G.; Clark, C. D.; Hoffman, M. Z.; Orizondo, P. L.; Perkovic, M. W.; Paul Rillema, D. P. Acid−Base and Electrochemical Properties of the MLCT Excited States and One-Electron-Reduced Forms of Ruthenium(II) Complexes Containing 2-(2'-Pyridyl)pyrimidine and 2,2'-Bipyridine in Aqueous Solution. *Inorg. Chem.* **1997**, *36*, 2252−2257.
(61) Anderson, P. A.; Anderson, R. F.; Furue, M.; Junk, P. C.; Keene, F. R.; Patterson, B. T.; Yeomans, B. D. Protonation Studies of Reduced Ruthenium(II) Complexes with Polypyridyl Ligands. *Inorg. Chem.* **2000**, *39*, 2721−2728.
(62) White, T. A.; Witt, S. E.; Li, Z.; Dunbar, K. R.; Turro, C. New $Rh_2(II,II)$ Architecture for the Catalytic Reduction of H^+. *Inorg. Chem.* **2015**, *54*, 10042−10048.
(63) Jencks, W. P.; Regenstein, J.*Handbook of Biochemistry and Molecular Biology*, 4th ed.; CRC Press: Boca Raton, 2010; pp 595−635.
(64) Sato, M.; Harata, A.; Hatano, Y.; Ogawa, T.; Kaieda, T.; Ohmukai, K.; Kawazumi, H. Acid-Base Equilibrium Constants and Distribution Coefficients of Aminopyrene between the Surface and Bulk of Liquid Water as Studied by a Laser Two-Photon Ionization Technique. *J. Phys. Chem. B* **2004**, *108*, 12111−12115.
(65) Klein, A.; Vogler, C.; Kaim, W. The δ in 18 + δ Electron Complexes: Importance of the Metal/Ligand Interface for the Substitutional Reactivity of "Re(0)" Complexes (α-diimine-)$ReI(CO)_3(X)$. *Organometallics* **1996**, *15*, 236−244.

https://doi.org/10.1021/acs.inorgchem.2c02400
Inorg. Chem. XXXX, XXX, XXX−XXX